



22 Icosahedrite, the first natural quasicrystal with composition  $\text{Al}_{63}\text{Cu}_{24}\text{Fe}_{13}$ , was discovered in  
23 several grains of the Khatyrka meteorite, a unique CV3 carbonaceous chondrite. The presence in  
24 the meteorite fragments of icosahedrite strictly associated with high-pressure phases like  
25 ahrensite and stishovite indicates a formation conditions at high pressures and temperatures,  
26 likely during an impact-induced shock occurred in contact with the reducing solar nebula gas. In  
27 contrast, previous experimental studies on the stability of synthetic icosahedral AlCuFe, which  
28 were limited to ambient pressure, indicated incongruent melting at  $\sim 1123$  K, while high-pressure  
29 experiments carried out at room temperature showed structural stability up to about 35 GPa.  
30 These data are insufficient to experimentally constrain the formation and stability of icosahedrite  
31 under extreme conditions. Here we present the results of *in situ* high pressure experiments using  
32 diamond anvil cells of the compressional behavior of synthetic icosahedrite up to  $\sim 50$  GPa at  
33 room temperature. Simultaneous high P-T experiments have been also carried out using both  
34 laser-heated diamond anvil cells combined with *in situ* synchrotron X-ray diffraction (at  $\sim 42$   
35 GPa) and multi-anvil apparatus (at 21 GPa) to investigate the structural evolution of icosahedral  
36  $\text{Al}_{63}\text{Cu}_{24}\text{Fe}_{13}$  and crystallization of possible coexisting phases. The results demonstrate that the  
37 quasiperiodic symmetry of icosahedrite is retained over the entire experimental pressure range  
38 explored. In addition, we show that pressure acts to stabilize the icosahedral symmetry at  
39 temperatures much higher than previously reported. Based on our experimental study, direct  
40 crystallization of Al-Cu-Fe quasicrystals from an unusual Al-Cu-rich melt would be possible but  
41 limited to a narrow temperature range beyond which crystalline phases would form, like those  
42 observed in the Khatyrka meteorite. An alternative mechanism would consist in late formation of  
43 the quasicrystal after crystallization and solid-solid reaction of Al-rich phases. In both cases,  
44 linking our results with observations in nature, quasicrystals are expected to preserve their

45 structure even after hypervelocity impacts that involve simultaneous high pressures and  
46 temperatures, thus proving their cosmic stability.

47 Keywords: Icosahedrite, Quasicrystals, CV3 chondrite, redox, Khatyrka meteorite, solar nebula.

## 48 **Introduction**

49 Quasicrystals (QC; Levine and Steinhardt 1984; Shechtman et al. 1984) represent a class of  
50 solids characterized by quasiperiodic translational order and forbidden rotational symmetries,  
51 such as the icosahedral (i) symmetry exhibited by  $Al_xCu_yFe_z$  alloys, where x varies between 61  
52 and 64, y is 24-26 and z 12-13 atomic% (Bancel 1999). This chemical interval corresponds to the  
53 compositional range at which the i-QC solely is stable up to  $\sim 1023$  K at ambient pressure. Above  
54 this temperature the stability field of the quasicrystal decreases to a very narrow chemical  
55 composition up to  $\sim 1123$  K, where the i-QC with composition  $Al_{62.5}Cu_{25}Fe_{12.5}$  coexists with a  
56 liquid + ( $\lambda$ ) monoclinic phase with composition  $Al_{13}Fe_4$  (Tsai 2013; Zhan and Lück 2003a-e). At  
57 temperature above  $\sim 1200$  K i-QC has been shown to be unstable, such that the liquid only  
58 coexists with the  $\lambda$  phase. At approximately 1300 K the system is totally molten and the liquid  
59 composition reflects that of the starting QC.

60 Experimental studies of the phase relationships at ambient pressure have been the only available  
61 tool available to date to constrain the origin of the first natural quasicrystal, icosahedrite  
62  $Al_{63}Cu_{24}Fe_{13}$  (Bindi et al. 2009). However, textural and petrographic evidence suggest that the  
63 natural quasicrystal formed in outer space under pressures and temperatures considerably higher  
64 than 1 bar and 1300 K (Bindi et al. 2012; Hollister et al. 2014). Recently, Stagno et al. (2014)  
65 performed *in situ* HP-HT X-ray diffraction studies and showed that the icosahedral symmetry of  
66 i-AlCuFe QC is retained at 5 GPa and temperature up to 1673 K. Above this temperature the

67 analogue of icosahedrite used for the experiments was found to decompose to a liquid in  
68 equilibrium with CuAl (corresponding to the mineral cupalite, an accessory phase also found in  
69 the Khatyrka meteorite), and the cubic  $\beta$  phase (Bindi et al. 2012). Although this study provided  
70 information on the compressional behavior of i-AlCuFe QC, the results gave only a lower-bound  
71 on the P-T stability of natural icosahedrite. Previous studies that focused on the compressional  
72 behavior and structural stability of QCs with compositions slightly different from that of  
73 icosahedrite include measurements on i-Al<sub>62</sub>Cu<sub>25.5</sub>Fe<sub>12.5</sub>, which was shown to be stable up to 35  
74 GPa (Sadoc et al. 1994, 1995; Lefebvre et al. 1995). The role of combined pressures and  
75 temperatures, however, remains to be explored.

76 Here we present experimental results using both diamond anvil cell (DAC) and multi-anvil  
77 techniques to investigate the stability of synthetic i-AlCuFe at higher pressure and temperature  
78 than those reported in previous studies. We show for the first time that the icosahedral structure  
79 is stabilized at high temperature as pressure increases, which makes quasicrystals behavior  
80 similar to that shown by crystalline materials when exposed to extreme conditions. Based on our  
81 results, icosahedrite might have formed within a large range of pressures and temperatures  
82 during the formation of our solar system under extremely reducing conditions, and Khatyrka  
83 might represent one of the many QC-bearing meteorites orbiting in our solar system or in other  
84 solar systems in the Milky Way and in galaxies throughout the cosmos.

## 85 **EXPERIMENTAL METHODS**

86 The synthetic icosahedral quasicrystal used as starting material was characterized by SEM and  
87 XRD measurements and shown to have the formula Al<sub>63</sub>Cu<sub>24</sub>Fe<sub>13</sub> (Bancel 1999) plus minor  
88 amounts of cupalite, (Cu, Fe)Al. The synthetic material was first broken in several small

89 fragments. A small cheap was, then, loaded in a diamond anvil cell with culet size of 600  $\mu\text{m}$  and  
90 crushed to a fine powder by hand loading. A small portion of the powder with dimensions of  
91 about  $30 \times 30 \mu\text{m}$  was picked with a needle and placed at the center of a symmetric diamond  
92 anvil cell with 300  $\mu\text{m}$  culet size using a Re gasket as sample chamber with a 150  $\mu\text{m}$  diameter  
93 hole. A couple of ruby spheres were placed next to the sample as pressure markers. One diamond  
94 anvil was supported by a cubic boron nitride (c-BN) backing plate, and the other anvil by a  
95 tungsten carbide (WC) backing plate. *In situ* angle-dispersive powder X-ray diffraction  
96 measurements were performed at high pressure at the 16BM-D beamline, HPCAT (APS,  
97 Argonne). The DAC was loaded with neon as pressure medium also used as pressure marker  
98 (Hemley et al. 1989), and mounted on a motor driven stage with the WC seat on the downstream  
99 side, and the c-BN seat on the upstream side. Pressures inside the DAC was measured with the  
100 ruby luminescence method (Mao et al. 1986) with an on-line system. The used wavelengths of  
101 the monochromatic incident X-ray beam was 0.42460  $\text{\AA}$  and 0.5166  $\text{\AA}$ , respectively. The beam  
102 was focused to a focal spot of  $5 \times 15 \mu\text{m}$  by using a pair of Kirkpatrick-Baez mirrors. The  
103 MAR345 image plate detector was placed at a distance approximately of 478 mm from the  
104 sample in order to obtain high resolution and accuracy of the Debye-Scherrer diffraction rings.  
105 Diffraction peaks were collected using a continuous  $\omega$ -oscillation scan mode over the range from  
106  $-6^\circ$  to  $+6^\circ$  with an exposure time of 180 seconds.

107 Simultaneous high-pressure and temperature synchrotron powder X-ray diffraction experiments  
108 were conducted at the 13ID-D beamline of GSECARS (APS, Argonne) using a focused  
109 monochromatic X-ray beam of 30 KeV and with wavelength of 0.4133  $\text{\AA}$ . Double-side laser  
110 heating was performed using two focused infrared laser beams on both sides of the sample co-  
111 axially aligned with the incoming X-ray beam using the X-ray induced luminescence on the

112 sample. Laser power was adjusted independently on upstream and downstream sides to control  
113 the measured temperature within  $\pm 100$ K. Heating durations at the target temperature was about  
114 10 min. Temperatures of the laser-heated sample were measured using thermal radiation spectra  
115 fitted to the blackbody radiation function (Prakapenka et al. 2008). Diffraction patterns were  
116 collected on a MarCCD-165 Detector with exposure time of 15 s. In these experiments chips of  
117 synthetic  $\text{Al}_{63}\text{Cu}_{24}\text{Fe}_{13}$  were also crushed and then slightly pressed to form a platelet. A small  
118 platelet with a diameter of approximately 60  $\mu\text{m}$  was loaded into the sample chamber of a  
119 symmetric diamond-anvil cell with flat anvils of 300  $\mu\text{m}$ -size culet. Pressure was measured using  
120 the thermal equation of state of Ne. The *in situ* X-ray diffraction patterns were processed using  
121 FIT2D software (Hammersley 1998), and the *d*-spacing relative to each reflection was accurately  
122 determined using PeakFit software.

123 Quench experiments were performed at 21 GPa and temperature between 1600 K and 2000 K  
124 using a 1500-ton Walker-type press available at the Carnegie Institution of Washington. The  
125 starting material used in this study is a synthetic icosahedral AlCuFe ( $\geq 99.9\%$ ) quasicrystalline  
126 powder with nominal composition of  $\text{Al}_{65}\text{Cu}_{23}\text{Fe}_{12}$  previously characterized (13). Tungsten  
127 carbide anvils of 3 mm truncation edge length (TEL) were used with 8 mm edge length MgO  
128 pressure media. Graphite and alumina capsules were used in the attempt to prevent oxidation of  
129 the starting material. The capsules were then placed in the central portion of a cylindrical Re  
130 furnace, surrounded by MgO sleeve and spacers. A  $\text{LaCrO}_3$  sleeve was used as thermal insulator  
131 outside the heater.

132 Details about the pressure calibration of the employed assemblies are reported in (Hirose and Fei  
133 2002). The temperature during the experiment at 1973 K was monitored with a W-5%Re/W-  
134 26%Re (C-type) thermocouple inserted within an alumina sleeve, with the junction in contact

135 with the top of the capsule. From this run a temperature versus power calibration curve was  
136 obtained and employed for the additional runs. The sample was compressed to the target pressure  
137 at a rate of 0.5 GPa/hr, then heated to the target temperature and kept manually constant within  
138 10 K for a period of 15-60 minutes. The sample was quenched by turning off the power to the  
139 furnace and, then, decompressed to ambient pressure.

140 All recovered samples from quench experiments were mounted in epoxy resin and polished  
141 parallel to the axial furnace direction for textural observation and chemical composition mapping  
142 by Field Emission Scanning Electron Microscope (JEOL JSM 6500F). Semi-quantitative  
143 analyses using energy-dispersive X-ray spectroscopy, we performed at 15 kV and 1.1 nA  
144 employing metals (Fe, Cu, Al,) and oxides ( $\text{Al}_2\text{O}_3$ ) as standards. Phase identification of the  
145 selected recovered run products was accomplished using an Oxford Diffraction Xcalibur PX  
146 Ultra single-crystal diffractometer fitted with a 165 mm diagonal Onyx CCD detector (CuK $\alpha$   
147 radiation). The crystal-to-detector distance was 7 cm. Data were processed using the CrysAlis  
148 software package version 1.171.31.2 (Oxford diffraction) running on the Xcalibur PX control  
149 PC.

150

## 151 **RESULTS AND DISCUSSIONS**

### 152 **Compressibility behavior of icosahedrite at high pressure**

153 Synthetic icosahedral quasicrystals with the formula  $\text{Al}_{63}\text{Cu}_{24}\text{Fe}_{13}$  (Bancel 1999) were used as  
154 starting materials for our *in situ* DAC experiments. An accurate textural and chemical analyses  
155 of the synthetic material showed minor amounts of (Cu, Fe)Al. The first set of experiments  
156 consisted of *in situ* powder angle-dispersive X-ray diffraction measurements on i-QC using

157 DACs up to  $\sim 50$  GPa at room temperature. These experiments aimed to investigate the evolution  
158 of the icosahedral structure under pressure, the determination of the lattice parameter and the  
159 equation of state. A total of 50 diffraction patterns were collected during compression and  
160 decompression ramps. Figure 1 shows a characteristic spotty diffraction pattern constantly  
161 observed during our experiments and resulting from heterogeneous size of the crystallites.  
162 Figure 2 shows the variation of the  $d$ -spacing for 7 known diffraction peaks with increasing  
163 pressure and after decompressing the sample to ambient pressure. The intensities of the peaks  
164 appear strongly affected by preferential orientation of the powder grains as also visible in Figure  
165 1. However, the shift in  $d$ -spacing with increasing pressure can be observed for most of the peaks  
166 up to the target pressure. In addition, the peak broadening is also visible as the pressure  
167 increases. After the sample was decompressed to ambient pressure, peaks appeared still  
168 broadened in agreement with what observed by Sadoc et al. (1994) for  $i\text{-Al}_{62}\text{Cu}_{25.5}\text{Fe}_{12.5}$ . The  
169 results indicate that high pressure favors the disorder of the atoms in the QC, without causing  
170 drastic rearrangements of the structure itself.

171 We collected additional diffraction patterns at higher resolution by moving the detector at the  
172 maximum distance from the sample ( $\sim 478$  mm). This allowed us to investigate more accurately  
173 the icosahedral structure, in particular the behavior in the high  $d$ -spacing region that included  
174 peaks (12,16) at  $5.53 \text{ \AA}$  and (8,4) at  $8.94 \text{ \AA}$ , respectively. For the indexing notation see Lu et al.  
175 (2001). The collected diffraction patterns are shown in Figure S1; although limited at pressures  
176 up to  $\sim 36$  GPa at room T, they clearly show the gradual broadening as pressure increases. Two  
177 additional peaks were also observed, with  $d$ -spacing of  $\sim 6 \text{ \AA}$  and  $9.7 \text{ \AA}$ , respectively, never  
178 reported so far for  $i\text{-AlCuFe}$ , that could be indexed using the automated identification scheme  
179 described by Lu et al. (2001) as (24,15) and (6,3), respectively. Our *in situ* X-ray diffraction

180 measurements show that no peaks appear or disappear up to the target pressure of ~50 GPa,  
181 which excludes possible pressure-induced phase transformations, including amorphization, as in  
182 the case of i-AlLiCu (Itie et al. 1996). The observed peak-broadening with pressure can be  
183 interpreted as arising from the increasing atomic disorder perhaps due to residual stress while  
184 preserving the icosahedral structure within the investigated pressure range.

185 We determined the pressure dependence of the lattice parameter  $a_{6D}$  up to the maximum pressure  
186 of ~50 GPa (see Table S1 of Supporting Information). The parameter is defined as,

187

$$188 \quad a_{6D} = d \sqrt{\frac{N + M\tau}{2(2 + \tau)}} \quad (1),$$

189

190 where  $d$  is the  $d$ -spacing in Å,  $N$  and  $M$  the Cahn indices for which the  $d$ -spacing is  
191 experimentally determined, and  $\tau$  is the golden ratio,  $(1+\sqrt{5})/2$  (Steurer and Deloudi 2009). The  
192 six-dimensional lattice parameter is shown to gradually decrease with increasing pressure (Fig.  
193 3). The slightly scattered data at 24-32 GPa is likely due to the less accurate pressure  
194 determination caused by the overlap between the (111) peak of Ne and the (80, 128) peak of i-  
195 AlCuFe. However, the lattice parameter calculated from compression experiments is in good  
196 agreement with that calculated on decompression. The estimated reduction of the lattice  
197 parameter from the ambient pressure value of 12.64 Å is about 8%. In addition, our  $a_{6D}$  value at  
198 5 GPa and room temperature is consistent with that determined by Stagno et al. (2014) at similar  
199 conditions. We conclude that the QC retains its icosahedral structure over the pressure range  
200 investigated. In addition, we point out that more specific experiments would be needed to claim  
201 the thermodynamic versus kinetic stability of icosahedrite. This note might be extended to most  
202 of the crystalline structures that have been investigated for decades using similar techniques, but

203 that in case of quasicrystals is of fundamental importance to understand their stability with  
204 respect to the possible alternative atomic configurations represented by amorphous and  
205 approximant phases (Tsai 2013). However, it remains still to be investigated whether these  
206 results confirm the stability of the i-QC under pressure or the transformation to a crystalline  
207 phase is too sluggish to be observed on the time scale of the experiment.

208 The zero pressure bulk modulus,  $K_0$ , and its pressure derivative  $K_0'$  were determined from the  
209 least-squares fit to several equation of state (EOS) models. We first discuss the fit to the first  
210 order Murnaghan EOS (Angel et al. 2014), which allows direct comparison with the results from  
211 previous studies in which the experimental data were treated using the same EOS model. This  
212 resulted in  $K_0 = 113.7(\pm 2.9)$  and  $K_0' = 4.22(\pm 0.22)$ , respectively. It can be seen from Figure 4 that  
213  $K_0$  and  $K_0'$  obtained from our data are slightly lower than those obtained for  $\text{Al}_{62}\text{Cu}_{25.5}\text{Fe}_{12.5}$  from  
214 previous authors using the same EOS, i.e.,  $139(\pm 6)$  GPa and 2.7 (Sadoc et al. 1994), and  
215  $155(\pm 10)$  GPa and 2 (Lefebvre et al. 1995). Our EOS parameters are also different from those  
216 determined for an approximant phase with composition  $\text{Al}_{64}\text{Cu}_{24}\text{Fe}_{12}$  that is close to our  
217 synthetic i-QC, with  $K_0$  and  $K_0'$  of  $175(\pm 16)$  GPa and 2.00 (Lefebvre et al. 1995). Such  
218 differences in the compressional behavior can be interpreted as due to either different  
219 composition of the QCs or distinct mechanical properties of the approximant (crystalline) phase.  
220 It should be kept in mind, however, that in previous studies in which DACs techniques were  
221 employed, silicon oil was used as a pressure medium, for which hydrostaticity is limited to very  
222 low pressure (Angel et al. 2007). Moreover, the previously suggested EOSs have been derived  
223 from data collected using energy-dispersive rather than angle-dispersive X-ray diffraction with  
224 the lattice parameter calculated using a different peak than the (8,4) used in this study without  
225 taking into consideration possible anisotropy of the material. Our experimental data were also fit

226 using either a third-order Birch-Murnaghan EOS [ $K_0 = 110.4(\pm 2.9)$  and  $K_0' = 4.79(\pm 0.28)$ ] and a  
227 Vinet et al. EOS [ $K_0 = 109.4(\pm 2.9)$  and  $K_0' = 5.06(\pm 0.29)$ ]. The new fitting models, although  
228 deviate slightly from the parameters obtained using a simple Murnaghan model, confirm the  
229 lower bulk modulus of synthetic icosahedrite with respect to the data currently available in  
230 literature. Finally, Figure 4 also shows the compressional behavior for pure *fcc*-Al, *fcc*-Cu  
231 (Dewaele et al. 2004) and *hcp*-Fe (Mao et al. 1990) plotted using the Vinet et al. and Birch-  
232 Murnaghan EOS models. For all these pure metals the structure has been reported to be stable for  
233 a wide pressure range  $> 100$  GPa. As observed by Sadoc et al. (1994), the compressional  
234 behavior of our synthetic icosahedrite is much closer to that of pure Cu, although Al represents  
235 the main constituent. We expect, therefore, a similar compressional behavior for i-AlCuFe  
236 quasicrystals varying in compositions according to the phase diagram proposed by Bancel  
237 (1999).

238

### 239 **Stability of the icosahedral symmetry at simultaneous high pressure and temperature**

240 Recently, the conditions for the formation of natural i-AlCuFe have been constrained on the  
241 basis of accurate textural and chemical analyses of the coexisting mineral phases within the  
242 CV3-like chondritic grains of the Khatyrka meteorite (Hollister et al. 2014; MacPherson et al.  
243 2013). The occurrence of rare alloys represented by the Al-Cu-Fe system along with the  
244 observation of melt droplets and phases such as stishovite and ahrensite have been referred to  
245 unusual petrological processes that likely occurred at simultaneous high pressures and  
246 temperatures generated by an impact shock. To shed light on the mechanisms of formation, a  
247 study of icosahedrite at high pressure and temperature could help to reach more definitive  
248 conclusions. A first study was done by Stagno et al. (2014) where the stability of synthetic

249 icosahedrite was observed *in situ* at 5 GPa up to  $\sim 1673$  K above which the sample was found to  
250 melt incongruently and produce two solid crystalline phases:  $\beta$ -phase and cupalite. These  
251 experiments, although limited to demonstrate the kinetic stability of icosahedrite, provided the  
252 first evidence that pressure might act to stabilize the QC at  $T$  higher than 1300 K.

253 *In situ* high P-T laser heating system diamond-anvil cell experiments were conducted to further  
254 constrain the stability field of icosahedrite. The synthetic quasicrystalline powder was first  
255 compressed to  $\sim 42$  GPa, then heated to  $\sim 1830$  K while collecting X-ray diffraction patterns to  
256 monitor any possible transformation or melting (see details in the Experimental Methods  
257 session). The sample was then cooled down to 1000 K before being quenched. The results show  
258 that during heating at about 1560 K the intensity of most of the peaks decreases dramatically,  
259 and new peaks always belonging to QC appear at  $d$ -spacing between 1.8 and 2.0 Å (Fig. 5).  
260 Interestingly, during cooling of the sample at about 1500 K the main peaks re-appear and are  
261 visible even after quenching the sample to room  $T$ . No amorphization or phase transformation  
262 was evident, and the new peaks characteristic of the QC become visible as a result of a strong  
263 preferential orientation. However, with increasing  $T$  the loss of quasicrystallinity (i.e., formation  
264 of crystal approximants) via a reversible process cannot be excluded.

265 The result of the high  $T$  run performed at the same pressure on a different point of the sample is  
266 shown in Fig. S2 (Supporting Information). In this case the QC was heated up to  $\sim 2110$  K and  
267 then quenched directly to room temperature. The results are similar to the previous experiment at  
268 1600 K, where peaks characteristic of synthetic icosahedrite are present. At higher temperature,  
269 however, new unknown peaks appear that are preserved also after quenching the sample to room  
270  $T$  suggesting that the i-QC might have decomposed irreversibly. *Ex situ* single crystal X-ray  
271 diffraction measurements on a micrometer-sized grain handpicked from the cell (see Fig. S3 of

272 Supporting Information) showed the 5-fold symmetry characteristic of i-QC. This result  
273 confirmed that the sample retained its structure, at least upon compression considering that it is  
274 difficult to establish whether or not the measured fragment was heated up to the target  
275 temperature.

276  
277 To address the above questions, we performed additional quench experiments using multi-anvil  
278 technique to better understand the nature of the unknown peaks discussed above. Experiments  
279 were performed at 21 GPa and temperature between 1673-1993 K using icosahedral AlCuFe  
280 ( $\geq 99.9\%$ ) quasicrystalline powder with nominal composition of  $\text{Al}_{65}\text{Cu}_{23}\text{Fe}_{12}$  previously  
281 characterized (Stagno et al. 2014).

282 SEM images using back-scattered electrons of the run products reveal the compositions and  
283 textures of the recovered material (Fig. 6). The run quenched from 1673 K consists of a single  
284 phase with composition  $\text{Al}_{64.11(\pm 0.66)}\text{Cu}_{24.70(\pm 0.74)}\text{Fe}_{11.19(\pm 0.22)}$ , which is consistent with the starting  
285 composition of the synthetic QC. Several grains showed a patchy texture that we believe are due  
286 to the onset of melting of the QC. At about 1773 K the recovered sample shows the coexistence  
287 of  $\beta$ -phase ( $\text{Al}_{64.73(\pm 0.36)}\text{Cu}_{20.23(\pm 0.91)}\text{Fe}_{15.04(\pm 0.68)}$ ), Fe-rich cupalite  
288 ( $\text{Al}_{48.77(\pm 0.35)}\text{Cu}_{36.10(\pm 0.93)}\text{Fe}_{15.13(\pm 0.70)}$ ) and a phase identified by the patchy texture with  
289 composition  $\text{Al}_{62.65(\pm 0.89)}\text{Cu}_{33.52(\pm 1.08)}\text{Fe}_{2.92(\pm 0.27)}$  that can be interpreted either as a Fe-poor  
290 khatyrkite or a melt. Small grains of  $\text{Al}_2\text{O}_3$  are also present and suggest possible oxidation of the  
291 material during the experiment. Finally, the recovered sample from 1973 K appears totally  
292 molten consisting of a Fe-rich liquid with composition  $\text{Al}_{12.07(\pm 0.50)}\text{Cu}_{21.34(\pm 1.04)}\text{Fe}_{65.48(\pm 0.73)}$  and  
293 with characteristic quench texture imposed by the presence of “skeletal” Al metal (Fig. 6d).

294 Results from quench experiments, therefore, would suggest 1) that the QC retains its stability at  
295 both high pressure and temperature and its icosahedral symmetry is also recoverable; 2) as  
296 temperature increases icosahedrite might melt congruently to, then, dissociate in a liquid with  
297 composition very similar to khatyrkite +  $\beta$ -phase + cupalite similarly to what reported by Stagno  
298 et al. (2014); 3) pure Al would be the first phase crystallizing from a liquid with icosahedrite-like  
299 composition.

300

### 301 **IMPLICATIONS**

302 Our results partially, but surprisingly, reproduce features observed in the Khatyrka meteorite in  
303 terms of phase assemblage (cupalite,  $\beta$ -phase, khatyrkite and pure Al) and texture, associated  
304 with the presence of icosahedrite. The coexistence of icosahedrite with a liquid having the same  
305 composition (i.e. congruent melting) than the ideal composition reported by Bancel (1999; i.e.,  
306  $\text{Al}_{63}\text{Cu}_{24}\text{Fe}_{13}$ ) has been never reported at such high pressure and would imply the i-QC being, at  
307 least, kinetically stabilized by entropy at high pressure to the point where the melting  
308 temperature is approached without transformation to any approximant phase. This would agree  
309 with the fast cooling rate crystallization model proposed by Hollister et al. (Hollister et al. 2014;  
310  $10^2$ - $10^3$  °C $s^{-1}$ ) from which the Al, Cu-rich assemblage formed. However, we point out that a  
311 similar mechanism of formation for icosahedrite appears unlikely as we assume here  
312 thermodynamic equilibrium between the QC and the liquid from which it forms. In fact, the  
313 coexistence of Al, Cu rich-phases with icosahedrite in the Khatyrka meteorite would suggest an  
314 initial high abundance of these elements, as confirmed by the finding of Al-rich Cu-bearing FeNi  
315 and sulfide phases in proximity of the QC. The finding of pure Al in our experiments is a further  
316 element of similarity with the natural assemblage (see Fig. 2 in Hollister et al. 2014) and can be

317 explained in light of its lower melting temperature with respect to Fe and Cu that would trigger  
318 its mobilization by diffusion mechanisms and exsolution. The presence of khatyrkite in our  
319 sample quenched at 1773 K with pure Al exsolved cannot be excluded and would represent a  
320 further evidence of the high-temperature regime occurred during crystallization of these phases  
321 even at pressures above 5 GPa within an extra-solar environment characterized by an unusual  
322 abundance of Al.

323 To date, two hypotheses have been proposed (Hollister et al. 2014) to explain the origin of Al-  
324 Cu-Fe alloys in the Khatyrka meteorite: 1) segregation from a silicate melt formed by an after-  
325 impact heating event and enriched in Al and Cu previously diffused-out from Fe-Ni alloy, and  
326 from which forsterite and diopside also could crystallize; 2) formation of Al-Cu metals during  
327 nebular processes before the impact occurred with re-melting and re-solidification of these  
328 alloys. Both scenarios appear as the result of multiple impact events that favored mechanisms  
329 such as diffusion, solid-solid reactions and oxidation-reduction with a further common feature  
330 represented by the initial high abundance of Cu and Al. It is, therefore, very unlikely that all  
331 these processes can be explained based on our experimental results. On the other hand, our  
332 experiments well reproduce the same phases observed in the meteoritic sample at higher  
333 pressures and temperatures than those proposed by Hollister et al. (2014), where a pressure of 5  
334 GPa and temperature of 1200 °C indicatively represent a lower-bound.

335 In conclusion, results from this study can be summarized as follows, 1) synthetic icosahedrite  
336 was shown to retain its structure up to ~50 GPa at ambient temperature; 2) it was experimentally  
337 demonstrated for the first time that pressure can stabilize the icosahedral Al-Cu-Fe quasicrystal  
338 at very high temperature until it melts with no evidence of phase transitions; 3) congruent  
339 melting of icosahedrite might be limited to a very narrow temperature interval beyond which Al,

340 Cu-rich phases would form. In addition, our results from quench experiments suggest that the  
341 bulk composition of the portion of solar nebula from which Khatyrka meteorite formed must  
342 have been much more enriched in Al and Cu than icosahedrite composition in case of single  
343 impact event followed by rapid solidification.

344 Based on our results the preservation of icosahedrite over cosmic time scales in a meteorite that  
345 formed at the early stage of the solar system results from its unexpected stability at high  
346 temperatures and pressures. Therefore, the presence of icosahedrite in other meteorites exposed  
347 to extreme conditions, but with similar bulk composition than Khatyrka, cannot be excluded.

348

#### 349 **Acknowledgments**

350 This work was partially supported by EFree, an Energy Frontier Research Center funded by the  
351 US DOE, Office of Science, Basic Energy funded under award DE-SC-000157 and award DE-  
352 NA-0006 and by CDAC under award DOE/NNSA. Part of this work was performed at  
353 GeoSoilEnviroCARS (Sector 13), Advanced Photon Source (APS), Argonne National  
354 Laboratory. GeoSoilEnviroCARS is supported by the National Science Foundation-Earth  
355 Sciences (EAR-1128799) and Department of Energy-GeoSciences (DEFG02-94ER14466). Part  
356 of this work were also performed at HPCAT (Sector 16), Advanced Photon Source (APS),  
357 Argonne National Laboratory. HPCAT operations are supported by DOE-NNSA under Award  
358 No. DE-NA0001974 and DOE-BES under Award No. DE-FG02-99ER45775, with partial  
359 instrumentation funding by NSF. The Advanced Photon Source is a U.S. Department of Energy  
360 (DOE) Office of Science User Facility operated for the DOE Office of Science by Argonne  
361 National Laboratory under Contract No. DE-AC02-06CH11357.

362

363 **References**

364 Angel, R.J., Bujak, M., Zhao, J., Gatta, G.D., Jacobsen, S.D. (2007) Effective hydrostatic limits  
365 of pressure media for high-pressure crystallographic studies. *Journal of Applied*  
366 *Crystallography*, 40, 26.

367 Angel, R.J., Gonzalez-Platas, J., Alvaro, M. (2014) EosFit7c and a Fortran module (library) for  
368 equation of state calculations. *Zeitschrift für Kristallographie*, 229, 405-419.

369 Bancel, P.A. (1999) Order and disorder in icosahedral alloys. *Quasicrystals*. In DiVincenzo D.P.  
370 and Steinhardt P.J., Eds, *Series on Directions in Condensed Matter Physics*, World  
371 Scientific, 16, 17–55.

372 Bindi, L., Steinhardt, P.J., Yao, N., Lu, P.J. (2009) Natural Quasicrystals. *Science*, 324, 1306–  
373 1309.

374 Bindi, L., Steinhardt, P.J., Yao, N., Lu, P.J. (2011) Icosahedrite,  $\text{Al}_{63}\text{Cu}_{24}\text{Fe}_{13}$ , the first natural  
375 quasicrystal. *American Mineralogist*, 96, 928-931.

376 Bindi, L., Eiler, J.M., Guan, Y., Hollister, L.S., MacPherson, G., Steinhardt, P.J., Yao, N. (2012)  
377 Evidence for the extraterrestrial origin of a natural quasicrystal. *Proceedings of the*  
378 *National Academy of Sciences*, 109, 1396–1401.

379 Dewaele, A., Loubeyre, P., Mezouar, M. (2004) Equations of state of six metals above 94 GPa.  
380 *Physical Review B*, 70(9), 094112.

381 Hammersley, A.P., (1998) FIT2D V12.077 Reference Manual, European Synchrotron Radiation  
382 Facility, Grenoble, France, Version 4.0.

383 Hemley, R.J., Zha, C.S., Jephcoat, A.P., Mao, H.-K., Finger, L.W., Cox, D.E. (1989) X-ray  
384 diffraction and equation of state of solid neon to 110 GPa. *Physical Review B*, 39(16),  
385 11820-11827.

386 Hirose, K. and Fei, Y. (2002) Subsolidus and melting phase relations of basaltic composition in  
387 the uppermost lower mantle. *Geochimica Cosmochimica et Acta*, 66, 2099-2108.

388 Hollister, L.S., Bindi, L., Yao, N., Poirier, G.R., Andronicos, C.L., MacPherson, G.J., Lin, C.,  
389 Distler, V.V., Eddy, M.P., Kostin, A., Kryachko, V., Steinhardt, W.M., Yudovskaya, M.,  
390 Eiler, J.M., Guan, Y., Clarke, J.J., Steinhardt, P.J. (2014) Impact-induced shock and the  
391 formation of natural quasicrystals in the early solar system. *Nature Communications*, 5, 1-8.

392 Itie, J.P., Lefebvre, S., Sadoc, A., Capitan, M.J., Bessiere, M., Calvayrac, Y., Polian, A. (1996)  
393 X-ray absorption and diffraction study of the stability of two quasicrystals (AlCuFe and  
394 AlCuLi) under high pressure. In C. Janot, and R. Mosseri, Eds., *Proceedings of the*  
395 *Fifth International Conference on Quasicrystals*, pp. 168. Singapore: World Scientific.

396 Janot, C. (1994) *Quasicrystals: A Primer*. Oxford University Press, Oxford.

397 Lefebvre, S., Bessière, M., Calvayrac, Y., Itie, J.P., Polian, A., Sadoc, A. (1995) Stability of  
398 icosahedral Al-Cu-Fe and two approximant phases under high pressure up to 35 GPa.  
399 *Philosophical Magazine B*, 72, 101–113.

400 Levine, D., and Steinhardt, P.J. (1984) Quasicrystals: A new class of ordered structures. *Physical*  
401 *Review Letter*, 53, 2477–2480.

402 Lu, P.J., Deffeyes, K., Steinhardt, P.J., Yao, N. (2001) Identifying and indexing icosahedral  
403 quasicrystals from powder diffraction patterns. *Physical Review Letter*, 87, 275507.

404 MacPherson, G.J., Andronicos, C.L., Bindi, L., Distler, V.V., Eddy, M.P., Eiler, J.M., Guan, Y.,  
405 Hollister, L.S., Kostin, A., Kryachko, V., Steinhardt, W.M., Yudovskaya, M.,

406 Steinhardt, P.J. (2013) Khatyrka, a new CV3 find from the Koryak Mountains, Eastern  
407 Russia. *Meteoritics and Planetary Science*, 48, 1499-1514.

408 Mao, H.-K., Xu, J., Bell, P.M. (1986) Calibration of the ruby pressure gauge to 800 kbar under  
409 quasi-hydrostatic conditions. *Journal of Geophysical Research*, 91(B5), 4673-4676.

410 Mao, H.-K., Wu, Y., Chen, L.C., Shu, J.F., Jephcoat, A.P. (1990) Static compression of iron to  
411 300 GPa and Fe<sub>0.8</sub>Ni<sub>0.2</sub> alloy to 260 GPa: Implications for composition of the  
412 core. *Journal of Geophysical Research*, 95(B13), 21737–21742.

413 Prakapenka, V.B., Kubo, A., Kuznetsov, A., Laskin, A., Shkurikhin, O., Dera, P., Rivers, M.L.,  
414 Sutton, S.R. (2008) Advanced flat top laser heating system for high pressure research at  
415 GSECARS: application to the melting behavior of germanium. *High Pressure Research*,  
416 28, 225-235.

417 Sadoc, A., Itie, J.P., Polian, A., Lefevbre, S., Bessi re, M., Calvayrac, Y. (1994) X-ray  
418 absorption and diffraction spectroscopy of icosahedral Al-Cu-Fe quasicrystals under high  
419 pressure. *Philosophical Magazine B*, 70, 855–866.

420 Sadoc, A., Itie, J.P., Polian, A., Lefevbre, S., Bessi re, M. (1995) Quasicrystals under high  
421 pressure. *Physica B*, 208-209, 495-496.

422 Shechtman, D., Blech, I., Gratias, D., Cahn, J. (1984) Metallic phase with long-range  
423 orientational order and no translational symmetry. *Physical Review Letter*, 53, 1951–1954.

424 Stagno, V., Bindi, L., Shibazaki, Y., Tange, Y., Higo, Y., Mao, H.-K., Steinhardt, P.J., Fei, Y.  
425 (2014) Icosahedral AlCuFe quasicrystal at high pressure and temperature and its  
426 implications for the stability of icosahedrite. *Scientific Reports*, 4, 5869.

427 Steurer, W., and Deloudi, S. (2009) *Crystallography of Quasicrystals. Concepts, Methods and*  
428 *Structures*. Springer, Berlin.

429 Tsai, A.P. (2013) Discovery of stable icosahedral quasicrystals: progress in understanding  
430 structure and properties. *Chemical Society Reviews*, 42, 5352–5365.

431 Zhang, L., and Lück, R. (2003a) Phase diagram of the Al-Cu-Fe quasicrystal-forming alloy  
432 system. I. Liquidus surface and phase equilibria with liquid. *Zeitschrift für Metallkunde*,  
433 94, 91–97.

434 Zhang, L., and Lück, R. (2003b) Phase diagram of the Al-Cu-Fe quasicrystal-forming alloy  
435 system. II. Liquidus surface and phase equilibria with liquid. *Zeitschrift für Metallkunde*,  
436 94, 98–107.

437 Zhang, L., and Lück, R. (2003c) Phase diagram of the Al-Cu-Fe quasicrystal-forming alloy  
438 system. III. Liquidus surface and phase equilibria with liquid. *Zeitschrift für Metallkunde*,  
439 94, 108–115.

440 Zhang, L., and Lück, R. (2003d) Phase diagram of the Al-Cu-Fe quasicrystal-forming alloy  
441 system. IV. Liquidus surface and phase equilibria with liquid. *Zeitschrift für Metallkunde*,  
442 94, 341–344.

443 Zhang, L., and Lück, R. (2003e) Phase diagram of the Al-Cu-Fe quasicrystal-forming alloy  
444 system. V. Solidification behavior of Al-Cu-Fe quasicrystal forming alloys. *Zeitschrift für*  
445 *Metallkunde*, 94, 774–781.

446

447

448

449 **Captions**

450 **Figure 1.** Representative powder X-ray diffraction pattern of  $i\text{-Al}_{64}\text{Cu}_{23}\text{Fe}_{13}$  compressed at high  
451 pressure. Texture and contribution from single crystals are typical features of the collected  
452 patterns. The Debye-Scherrer rings were labeled as in case of QCs using the two-integer indexes  
453 by Janot (1994). The diffraction patterns were processed using Fit2D (Hammersley 1998) and  
454 Peakfit softwares.

455  
456 **Figure 2.** Pressure dependence of the powder X-ray diffraction patterns of  $i\text{-QC}$  collected at  
457 room temperature in angle-dispersive mode (wavelength of  $0.4246 \text{ \AA}$ ). Filled circles indicate  
458 peaks of ruby (pressure marker), grey circles for Au (pressure marker), empty circles for Re  
459 (gasket) filled triangles for Ne (pressure medium). The diffraction peaks were indexed using  
460 Cahn indices ( $N, M$ ) following the scheme proposed by Janot (1994; see also Steurer and  
461 Deloudi 2009).

462  
463 **Figure 3.** Variation of the lattice parameter as function of pressure. Notes: yellow square,  
464 ambient pressure value (Bindi et al. 2011); black and white squares, lattice parameter determined  
465 respectively from compression and decompression experiments; gray squares, experiments at  
466 higher resolution.

467 **Figure 4.** Pressure-volume relations for  $i\text{-Al}_{64}\text{Cu}_{23}\text{Fe}_{13}$  with experimental data (black squares)  
468 fitted using a Murnaghan EOS (dashed black line). Results from Birch-Murnaghan and Vinet et  
469 al. EOS fits are here omitted since both closely overlapped to the Murnaghan EOS fit.  
470 Uncertainties are within the symbol size. Our fit is compared with previous studies by Sadoc et  
471 al. (1994; gray line) and Lefbvre et al. (1995; blue line) both for icosahedral  $\text{Al}_{62}\text{Cu}_{25.5}\text{Fe}_{12.5}$  and  
472 for one approximant phase with composition  $\text{Al}_{64}\text{Cu}_{24}\text{Fe}_{12}$  (Lefbvre et al. 1995; yellow line). The

473 two curves obtained from these previous studies are extrapolated up to 52 GPa assuming that no  
474 structural phase transformation occurs. The EOS of pure Al, Cu (Dewaele et al. 2004) and Fe  
475 (Mao et al. 1990) are also reported with green, blue and brown, respectively.

476 **Figure 5.** Representative angle-dispersive (wavelength of 0.4133 Å) X-ray diffraction patterns  
477 for synthetic icosahedrite as function of temperature at ~ 42 GPa. Diffraction patterns were  
478 collected with 15s exposure time after keeping the sample at approximately constant  $T$  for 180s.  
479 Peaks are indexed as mentioned above. Filled black triangles indicate the (111) and (200) peaks  
480 of Ne pressure medium. a) Shown is the stability of i-QC during heating up to about 1830 K  
481 followed by slow cooling down to 1000 K before quench.

482 **Figure 6.** Back-scattered electron (BSE) images of the recovered sample from runs at 21 GPa. a)  
483 Run at 1673 K showing the presence of i-QC also confirmed by the five-fold symmetry in (b)  
484 using single crystal X-ray diffraction. (c) Recovered sample from 21 GPa and 1773 K and d)  
485 1973 K, respectively.

486

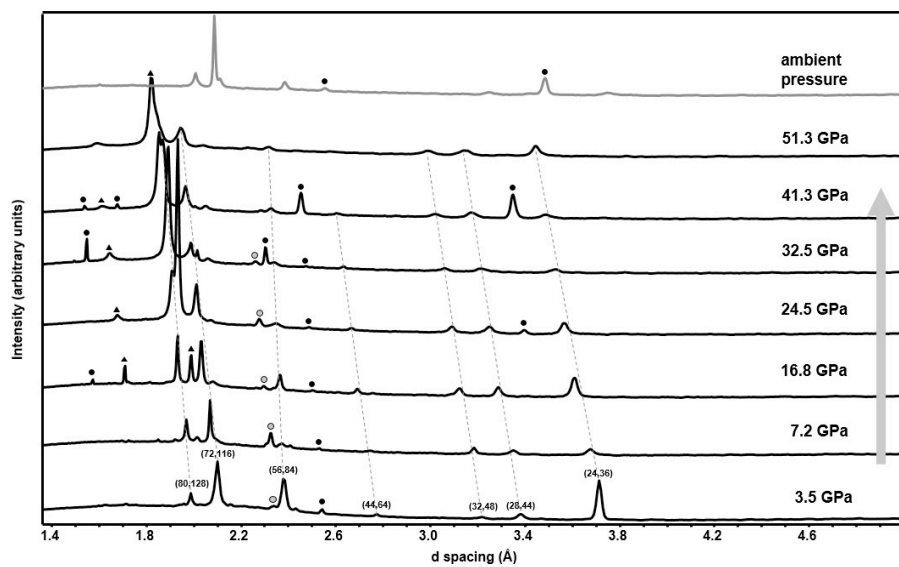
487 **Figures**

488



489

Figure 1

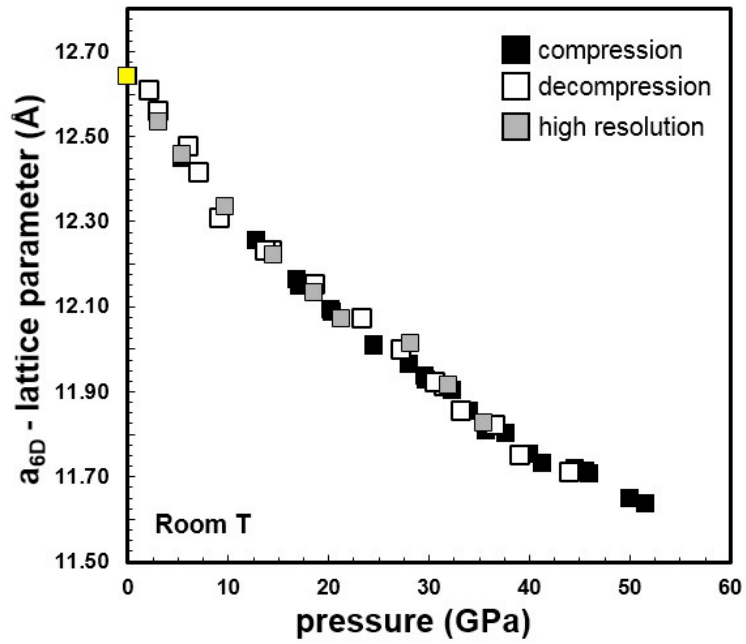


490

491

Figure 2

492

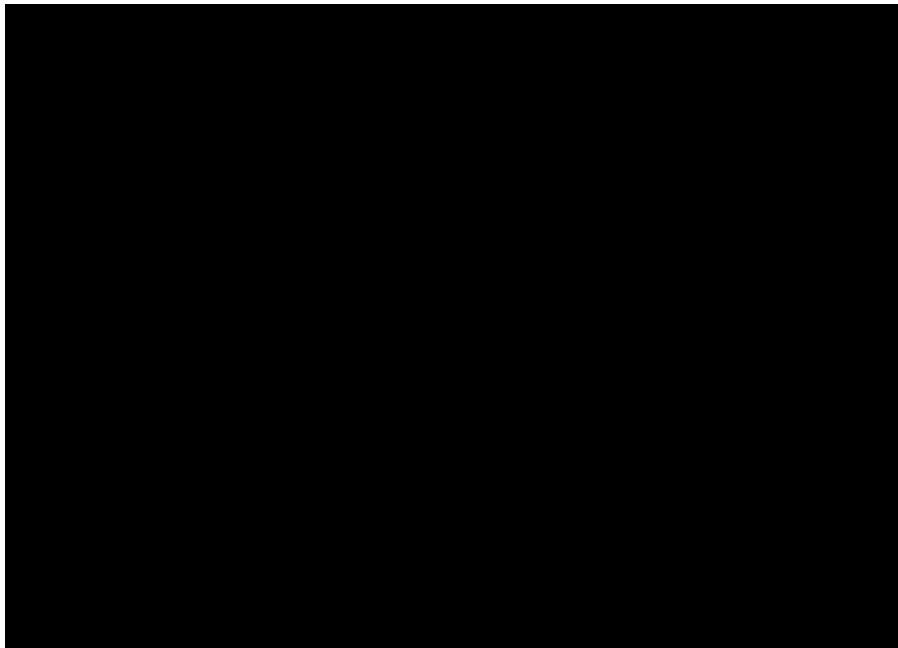


493

494

495

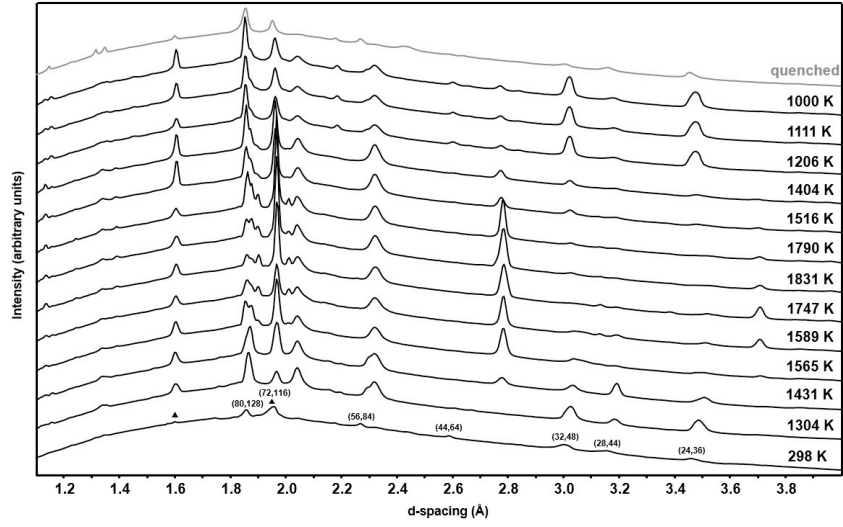
Figure 3



496

497

Figure 4



498

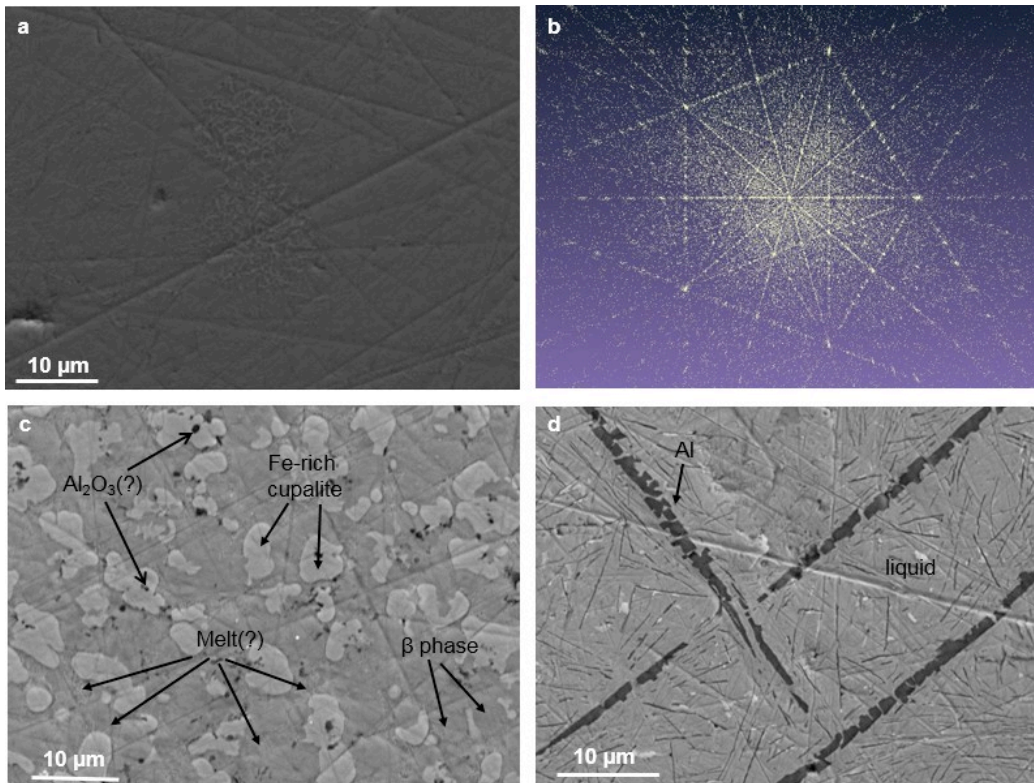
499

500

501

502

Figure 5



503

504

Figure 6